Microstructural properties of (Fe, Co)SiBCuNb nanocrystalline alloys

2002 J. Phys.: Condens. Matter 14 883

(http://iopscience.iop.org/0953-8984/14/4/321)

INSTITUTE OF PHYSICS PUBLISHING JOURNAL OF PHYSICS: CONDENSED MATTER

J. Phys.: Condens. Matter **14** (2002) 883–893 PII: S0953-8984(02)26759-4

Microstructural properties of (Fe, Co)SiBCuNb nanocrystalline alloys

J M Borrego[1], C F Conde[1], A Conde[1] and J M Greneche[2]

[1] Departamento de Física de la Materia Condensada, Instituto de Ciencia de Materiales CSIC—Universidad de Sevilla, Apartado 1065-41080, Sevilla, Spain
[2] Laboratoire de Physique de l'Etat Condensé, UMR CNRS 6087, Université du Maine, F-72085 Le Mans Cédex 9, France

E-mail: conde@cica.es

Received 6 July 2001, in final form 25 October 2001
Published 18 January 2002
Online at stacks.iop.org/JPhysCM/14/883

Abstract

$Fe_{73.5-x}Co_xSi_{13.5}B_9Cu_1Nb_3$ ($x = 13.5$ and 60 at.%) nanocrystalline alloys were studied by means of x-ray diffraction, ^{57}Fe Mössbauer spectrometry and thermomagnetic measurements. For the first time, the compositions of both the Fe, Co, Si nanocrystalline and the residual amorphous phases were determined on the basis of combined structural and magnetic hyperfine data. The Co content of the nanocrystalline phase was found to be the same as the Co content of the as-cast alloy. The hyperfine magnetic field distribution of the intergranular phase shows the emergence of a bimodal behaviour, consistent with a two-cluster-like model. Such behaviour is attributed to the presence of iron-rich and iron-poor zones located in the bulk of the intergranular region and at the periphery of the crystalline grains, respectively.

1. Introduction

Nanocrystalline Fe-based alloys are interesting materials not only from the fundamental point of view due to their original structural and magnetic properties, but also because of their industrial potential due to their excellent soft magnetic properties, combining high saturation magnetic flux and high permeability [1, 2]. The most studied system is based on FeSiB amorphous alloys containing Cu and Nb, the typical example being the $Fe_{73.5}Si_{13.5}B_9Nb_3Cu_1$ alloy, known as Finemet [3]. The microstructure of these alloys, obtained by controlled crystallization of the amorphous precursor, consists of nanometre-size Fe, Si grains embedded in a residual amorphous matrix. Their excellent properties as soft magnetic materials are strongly dependent on this particular nanostructure, the relevant parameters being the crystalline volume fraction, the size of the crystals and the composition of both the nanocrystalline and the residual amorphous phases.

It is well established that small changes of composition can significantly modify the magnetic properties. Thus, the substitution of Co for Fe in nanocrystalline alloys represents an interesting topic due to the possibility of improving the already excellent soft magnetic properties of these alloys [4, 5]. In recent years FeCoMB(Cu) nanocrystalline alloys, known as HITPERM, have excited great interest in extending their soft magnetic behaviour to higher temperatures [6]. So, they represent a good choice for high-temperature applications. In this paper the effect of partial replacement of Fe by Co on the nanocrystallization process of $Fe_{73.5-x}Co_xSi_{13.5}B_9Cu_1Nb_3$ ($x = 13.5$ and 60) alloys is studied by means of x-ray diffraction (XRD), Mössbauer spectrometry (MS) and thermomagnetic measurements (TMG). These results will be compared with those obtained previously on Co-free nanocrystalline alloys [7]. Study of the composition of the crystalline Fe, Co, Si grains requires the combination of Mössbauer and XRD data. Indeed, they allow the estimation of the Fe atomic crystalline fraction and the Si content of the grains, and the determination of the lattice parameter and the volume fraction of the crystalline phase, respectively. We recently proposed for the first time such an approach [8]. It is also important to emphasize that, to our knowledge, very few studies on Co-containing nanocrystalline alloys based on the combination of different techniques have yet been reported in literature.

The process of devitrification of both alloys has been reported previously [9]. It takes place through two main stages, exhibiting the typical features found for Finemet-type alloys. The first step results in the formation of metal-rich Fe, Co, Si nanocrystals with a mean size of about 12 nm for the Fe-rich alloy and 20 nm for the Co-rich alloy, embedded in a residual amorphous matrix. The substitution of 13.5 at.% Co for Fe stabilizes the amorphous alloy, increasing its crystallization temperature by about 20 K with respect to the Co-free alloy. In contrast, the crystallization onset temperature decreases by about 40 K for the Co-rich alloy.

2. Experimental procedure

Amorphous ribbons, 6 mm wide and 25 μm thick, with nominal compositions $Fe_{73.5-x}Co_xSi_{13.5}B_9Cu_1Nb_3$ ($x = 13.5$ and 60) were obtained by a single-roller melt-spinning technique. TMG were made in a thermobalance with the magnetic field of a small magnet ($\sim$15 mT) applied to the sample. The previous calibration of the thermobalance (Perkin–Elmer TGA-7) was checked by using the Curie points of nickel, Perkalloy and iron standards. Values of the Curie temperature, T_C, of the amorphous phase were determined from the intersection point of the steepest tangent to the TMG curve with the T-axis or with the magnetization curve extrapolated down to temperatures $T < T_C$.

Mössbauer spectra were taken in transmission geometry using a constant-acceleration spectrometer with a ^{57}Co(Rh) source. The spectra were recorded with the γ-beam perpendicularly oriented to the ribbon plane at room temperature. Mössbauer spectra were fitted with the NORMOS [10] program. Some aspects of the fitting procedure have been widely discussed for spectra of iron-based nanocrystalline alloys [11, 12]. The isomer shift values, δ, are quoted relative to α-Fe at 300 K.

Thermal treatments of the samples for XRD, MS and TMG studies were performed under an Ar atmosphere in a halogen lamp furnace. The amorphous samples were annealed at a temperature $\sim$30 K below the respective crystallization onset, T_{onset} (table 1), for 16, 45, 256 and 480 min and at a temperature $\sim$10 K below T_{onset} for 330 min. Due to the difficulty of implementing the fitting methods for both XRD patterns and Mössbauer spectra when the crystalline or the amorphous component predominates (i.e. the crystalline fraction is very high or very low), we restrict our discussion to crystalline fractions ranging from 15 to 65%.

Table 1. Crystallization onset and Curie temperatures of $Fe_{73.5-x}Co_xSi_{13.5}B_9Cu_1Nb_3$ as-quenched alloys, and structural parameters of nanocrystalline and intergranular phases in nanocrystalline samples.

x	T_{onset} (K) ±5	T_C (K) ±5	a (Å) ±0.002	$\langle d \rangle$ (nm) ±2	x_m (Å) ±0.02
0	791	600	2.838	12	2.50
13.5	805	635	2.834	12	2.50
60	754	675	2.824	20	2.47

3. Results and discussion

3.1. X-ray diffraction

The structural evolution of the Fe, Co, Si phase was studied from samples annealed at different temperatures and for different times to obtain different crystalline fractions. The volume fraction of the nanocrystalline phase, x_c, was obtained from the integral intensities of the (110) reflection of the crystalline phase and that of the first diffuse maximum of the amorphous phase fitted by pseudo-Voigt functions [13]. It should be noted that the error in the estimation of the crystalline fraction due to not considering the difference between the scattering power of the crystalline and amorphous phases is negligible in comparison to the error inherent to the deconvolution procedure.

The lattice parameter, a, of the Fe, Co, Si phase, calculated from the angular position of the (110) reflection and the mean size of the nanocrystals, $\langle d \rangle$, estimated using Scherrer's equation, were found to be almost constant during the nanocrystallization process for x_c-values above 15 at.%. As shown in table 1, the lattice parameter decreases as the Co content of the amorphous alloy increases. The composition of the nanocrystalline phase ($Fe_{80}Si_{20}$) is easy to obtain for the Co-free alloy from the linear dependence of the lattice parameter with Si content in Fe, Si alloys [14], assuming that the other constituents are nearly insoluble in Fe [15]. However, for the estimation of the grain composition in Co-containing alloys it will be necessary to use MS data. The mean size of the crystalline grains derived from x-ray data (table 1) increases with the Co content of the alloy. These values agree with those obtained from transmission electron microscopy (TEM) [9].

The angular position of the first amorphous maximum was used to determine the average interatomic distance in the first TM–TM (TM, transition metal) coordination shell of the amorphous phase, x_m. It may be noted that x_m (table 1) decreases as the Co concentration increases, in agreement with the results found for $(Fe_{1-x}Co_x)_{85}B_{15}$ alloys [16].

3.2. Mössbauer spectrometry

3.2.1. Amorphous alloys. Mössbauer spectra of as-quenched samples (figure 1(a)) were fitted using a discrete hyperfine magnetic field distribution, $P(B)$, typical of the amorphous structure. In order to reproduce the asymmetrical shape of the spectra, it was necessary to introduce a linear correlation between the magnetic hyperfine field and the isomer shift [17] of the components of the distribution. Table 2 lists the mean values of the hyperfine parameters.

The mean hyperfine magnetic field, $\langle B \rangle$, shows a nearly linear increase with the Co content of the alloy. The same behaviour is found for the magnetic moment per transition metal in $(Fe_xCo_{100-x})_{73}Si_{17}B_{10}$ and $(Fe_xCo_{100-x})_{76.7}Si_{13.3}B_{10}$ alloys and can be explained, as a first approximation, in terms of a simple rigid-band model [18]. Our results contrast with those reported for $(Fe_{1-x}Co_x)_{80}B_{20}$ [19], $(Fe_xCo_{1-x})_{77}Si_{10}B_{13}$ [20] and $Fe_xCo_{78-x}Si_9B_{13}$ [21]

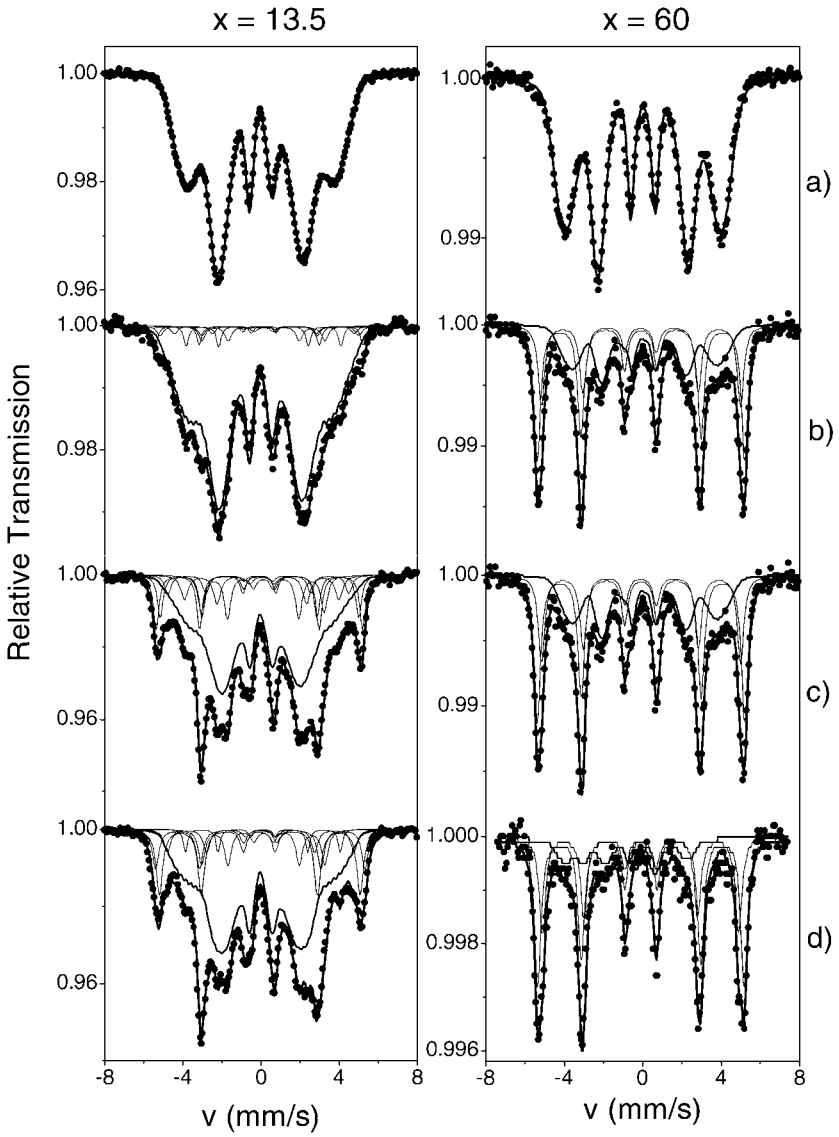

Figure 1. Transmission Mössbauer spectra and their fitting for $Fe_{73.5-x}Co_xSi_{13.5}B_9Cu_1Nb_3$ samples: (a) as-quenched, (b) annealed at a temperature ∼30 K below their respective crystallization onset for 45 min and (c) for 480 min and (d) at a temperature ∼10 K below their respective crystallization onset for 330 min.

alloys, for which $\langle B \rangle$ is nearly independent of the Co content, and those for $Fe_{85-x}Co_xB_{15}$ alloy [22] for which $\langle B \rangle$ does not show a monotonic variation.

The isomer shift, δ, increases with the Co concentration (table 2). This result is consistent with those found for $(Fe_xCo_{1-x})_{80}B_{20}$ [19], $(Fe_xCo_{1-x})_{77}Si_{10}B_{13}$ [20], $Fe_xCo_{78-x}Si_9B_{13}$ [21], $Fe_{85-x}Co_xB_{15}$ [22] and $(Fe_xCo_{1-x})_{75}Si_{15}B_{10}$ [23] alloys. It can also be roughly explained in the frame of the rigid-band model as due to an increase of the 3d electron density at the Fe sites due to the Co, which contributes with one 3d electron more than Fe, but a more complete explanation should take topological effects into account [24].

Table 2. Mean hyperfine parameters of $Fe_{73.5-x}Co_xSi_{13.5}B_9Cu_1Nb_3$ as-quenched samples. ('Std' stands for 'standard deviation'.)

x	$\langle B\rangle$ (T) ±0.5	Std (T) ±0.5	$\langle\delta\rangle$ (mm s^{-1}) ±0.01	2ε (mm s^{-1}) ±0.01	$\langle\theta\rangle$ (deg) ±3
0	20.6	5.0	0.10	−0.02	67
13.5	21.5	5.0	0.11	−0.02	69
60	24.0	4.2	0.17	−0.02	61

The hyperfine magnetic field distributions shown in figure 2 reveal the presence of an intense peak around 22 T for the alloys with $x = 0$ and 13.5 and around 24 T for the alloy with $x = 60$ and a small tail at low hyperfine field values (∼12 T) for the three compositions. It can also be observed that $P(B)$ for the alloy with $x = 60$ is clearly narrower that those corresponding to alloys with $x = 0$ and 13.5. The same tendency is found for the standard deviation, Std (table 2). A similar decrease of Std is found in $Fe_{85-x}Co_xB_{15}$ [16, 22], $(Fe_xCo_{1-x})_{77}Si_{10}B_{13}$ [20], $Fe_xCo_{78-x}Si_9B_{13}$ [21] and $(Fe_xCo_{1-x})_{75}Si_{15}B_{10}$ [25] alloys.

The standard deviation is related to the width of the distribution of exchange interactions between Fe atoms and magnetic atoms located in their neighbourhood. The width of this distribution depends on both the topological short-range order (SRO) of metallic atoms around Fe, and the chemical SRO, sensitive to the composition, that takes into account the probability of distribution of the different type of magnetic atoms around the Fe one as well as the presence of metalloid atoms. An increase of both topological and chemical short-range order around Fe atoms will cause a decrease of the standard deviation. Therefore, our results allow us to conclude that the increase of Co content in FeCoSiBNbCu systems leads to an increase of the short-range order around the Fe atoms, resulting in larger values of B and narrower $P(B)$.

The magnetic anisotropy of the as-quenched samples can be derived from the relative intensities of the absorption lines 2 and 3, from which the value of θ, defined by the directions of the hyperfine field and of the γ-rays, can be obtained. The values of θ (table 2) indicate the presence of an in-plane texture of magnetic domains for the three alloys, being more clearly evidenced for the alloys with $x = 0$ and 13.5. This preferential orientation is consistent with the presence of large quenched-in stresses.

3.2.2. Nanocrystalline alloys. Mössbauer spectra of the annealed samples (figure 1) exhibit a complex hyperfine structure and significant differences can be observed between the spectra of the two alloys. The sharp lines from the crystalline phase, that appear superimposed with the broad overlapped lines attributed to the residual amorphous matrix, were fitted using five and two discrete magnetic subspectra for the samples with $x = 13.5$ and 60, respectively. They are attributed to DO_3 Fe, Co, Si and to bcc Fe, Co, Si phases, respectively [26, 27].

The Fe atomic fraction of the nanograins, x_{MS}, was determined from the crystalline and amorphous absorption areas, assuming the same value of the f recoilless factor for both iron-containing phases. The Si content of the nanograins (18 ± 2 and 5 ± 2 at.% for $x = 13.5$ and 60, respectively) was estimated from the number of Fe sites and the proportion of each Fe component corresponding to the crystalline phase (table 3) [26–28]. In particular, in the case of the Fe-rich alloys, the Si content was evaluated from the relative area of the sites A_4 and $A_7 + A_8 + D$ [12, 29]. The lack of accuracy of these values is due to the complexity of the hyperfine structure.

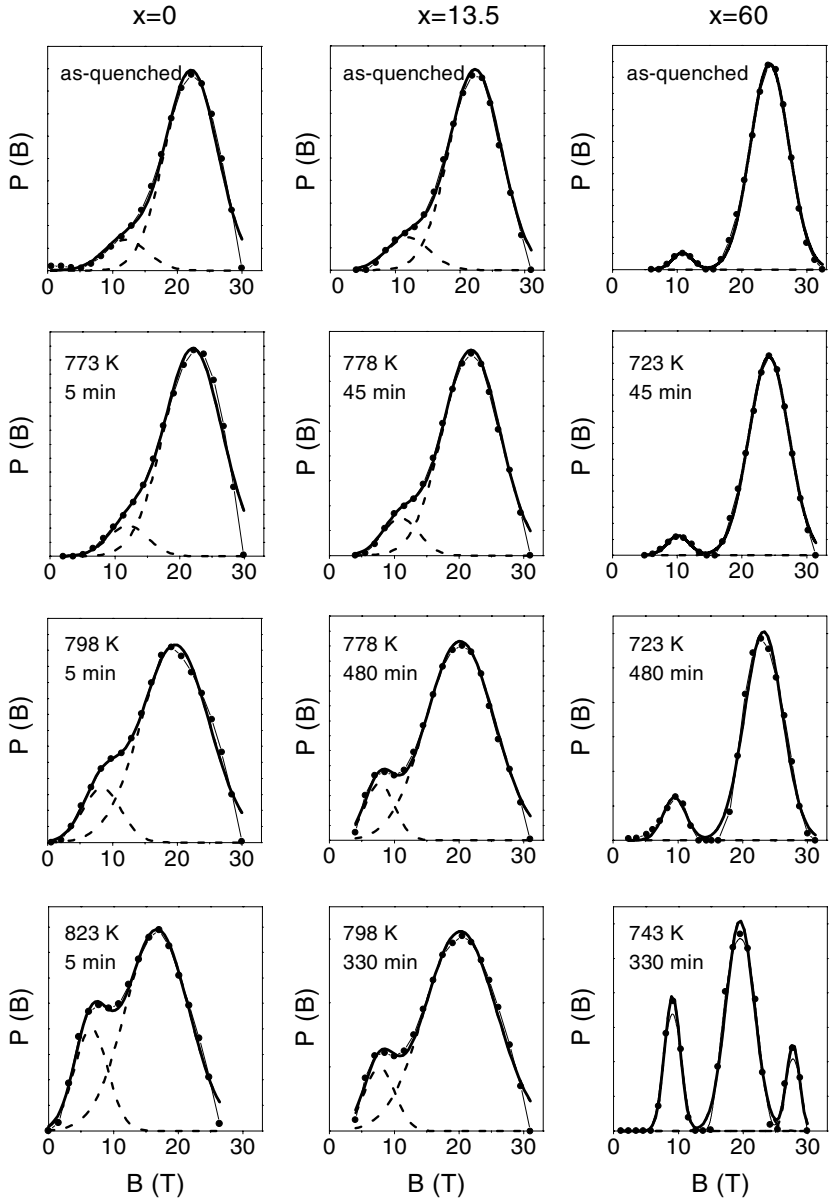

Figure 2. Hyperfine magnetic field distributions characteristic of the amorphous phase for as-cast and nanocrystalline samples annealed under different conditions. The $P(B)$ values are relative to the amorphous component.

The content (atomic percentage) of element i in the as-quenched, crystalline and residual amorphous phases, $(x_i)_{\mathrm{asq}}$, $(x_i)_{\mathrm{cr}}$ and $(x_i)_{\mathrm{am}}$, respectively, will have to satisfy the closure relation:

$$(1 - x_{\mathrm{c}})(x_i)_{\mathrm{am}} + x_{\mathrm{c}}(x_i)_{\mathrm{cr}} = (x_i)_{\mathrm{asq}}. \tag{1}$$

The compositions of the nanocrystals that fulfil all the above requirements are $Fe_{68.5}Co_{13.5}Si_{18}$ for $x = 13.5$ and $Fe_{35}Co_{60}Si_5$ for $x = 60$. The lattice parameter provides

Table 3. Hyperfine field, B, and relative intensities of the different Fe sites corresponding to the nanocrystalline grains, I, as a function of Co content (at.%) for $Fe_{73.5-x}Co_xSi_{13.5}B_9Cu_1Nb_3$ alloys with a crystalline fraction of about 35%.

	$x = 0$		$x = 13.5$		$x = 60$	
Site	B (T) ±0.5	I (at.%) ±5	B (T) ±0.5	I (at.%) ±5	B (T) ±0.5	I (at.%) ±5
A_8+D	32.2	25	32.8	28	32.9	58
A_7	30.9	15	31.6	23	31.5	42
A_6	28.6	24	28.9	11	—	—
A_5	24.5	15	24.6	16	—	—
A_4	19.5	21	19.3	22	—	—

an additional confirmation for the proposed crystalline composition [14]. The Co content of the nanocrystalline phase turns out to be the same as the nominal Co concentration; therefore the Co content in the intergranular phase remains unchanged during the nanocrystallization process, at least for crystalline fraction ranging from 15 to 65%. Similar results are found by Mössbauer measurements on $(Fe_{100-y}Co_y)_2B$ alloys [30] and by atom probe field-ion microscopy (APFIM) in FeCoBNbCu alloys [31].

The average hyperfine magnetic field of the crystalline component, that remains constant for the crystalline fractions considered, increases linearly with the Co content of the grains.

Table 4 lists the values of the volume crystalline fraction, x_c, and of the Fe atomic fraction of the nanograins, x_{MS}, for nanocrystalline alloys estimated at different stages of the nanocrystallization process. It can be observed that for the alloys with $x = 0$ and 13.5 the two quantities are almost equal, considering their error bars. This result justifies calculating the crystalline fraction of nanocrystalline alloys from the relative absorption areas of Mössbauer subspectra of both crystalline and amorphous components. In contrast, for the alloy with $x = 60$, a significant difference between the x_c- and x_{MS}-values is found. This discrepancy originates from the significantly higher Fe content of the nanocrystals with respect to that of the amorphous matrix.

The estimated composition of the intergranular amorphous phase, obtained from equation (1), as a function of the crystalline fraction is shown in figure 3. Fe content decreases monotonically with x_c for all the alloys, while Si content decreases with x_c for $x = 0$ and 13.5 but increases for $x = 60$. This change in Si concentration would affect to the Curie temperature of the remaining amorphous phase in these alloys. An increase with x_c of the B and Nb content of the amorphous phase is found in all the alloys.

The mean hyperfine field of the amorphous phase, $\langle B \rangle_{am}$, decreases monotonically with x_c for the three alloys (figure 4) and a linear dependence of $\langle B \rangle_{am}$ on the Fe content of the amorphous phase is found.

The hyperfine magnetic field distributions corresponding to the amorphous phase (figure 2) exhibit a bimodal behaviour which can be roughly described by means of two Gaussian components, consistent with a two-cluster-like model. The structure of the as-quenched alloy induces an intrinsic bimodal behaviour as previously suggested in [32], although poorly defined. This feature becomes more pronounced as the nanocrystallization progresses, and it can be interpreted as due to the emergence of two magnetically distinct types of iron site within the intergranular phase, associated with the crystallization process. High-field values can be attributed to Fe atoms which are preferentially surrounded by Fe, Co, Si and B atoms as nearest neighbours whereas the low-field component is ascribed to those surrounded by Nb and B.

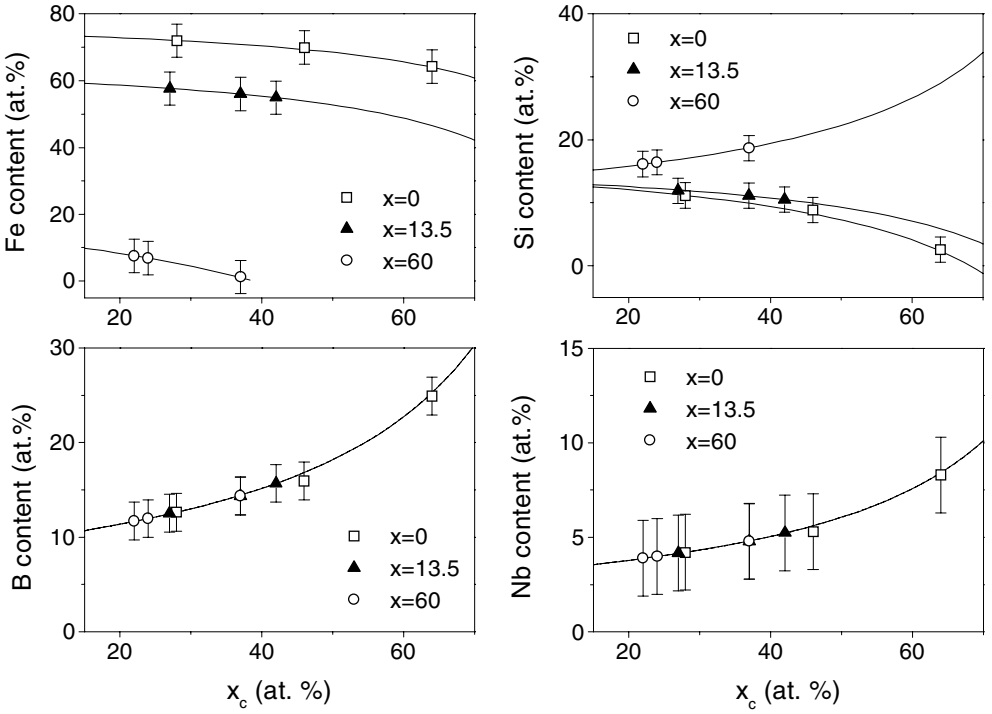

Figure 3. Composition of the intergranular phase as a function of the crystalline fraction obtained from equation (1) in the text, for $Fe_{73.5-x}Co_xSi_{13.5}B_9Cu_1Nb_3$ ($x = 0$, 13.5 and 60) alloys. The symbols represent the experimental data.

Table 4. Volume crystalline fraction, x_c (at.%), and Fe-atom fraction of the nanograins, x_{MS} (at.%), as a function of the annealing treatment: annealing temperature, T_a (K), and annealing time, t_a (min). The estimated error is ±5 at.% for all the calculated values.

$x = 0$			$x = 13.5$			$x = 60$		
T_a			T_a			T_a		
t_a	x_c	x_{MS}	t_a	x_c	x_{MS}	t_a	x_c	x_{MS}
773	11	13	723	13	15	778	12	30
5			45			45		
753	28	32	723	28	32	778	25	58
60			256			256		
525	47	54	723	38	42	778	25	62
5			480			480		
823	65	75	743	43	47	798	35	80
60			330			330		

Indeed, the high-field peak value is close to that found in FeB and FeSiB amorphous alloys [33]. The atomic diffusion mechanisms which occur during the nanocrystallization process favour the formation of a non-homogeneous chemical amorphous matrix. The number of constituents and their different diffusivities make difficult a clear interpretation of the hyperfine field distribution. Nevertheless high contents of refractory-element Nb and B atoms have been evidenced by APFIM at the periphery of crystalline grains in Finemet alloys, which prevent the growth of grains [34]. Consequently the present low-field component could be attributed to

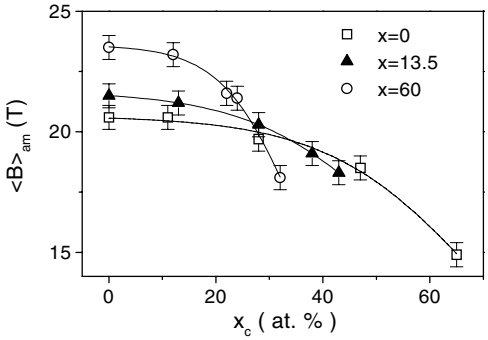

Figure 4. Mean hyperfine field of the intergranular phase as a function of the crystalline fraction.

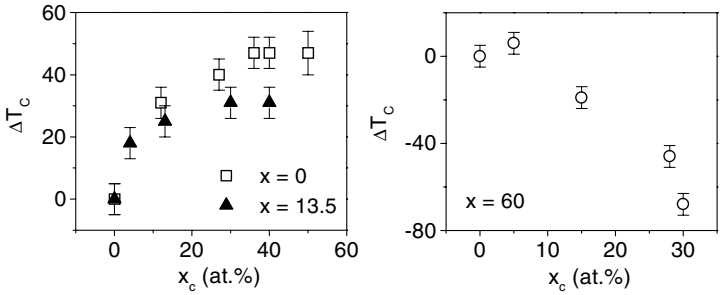

Figure 5. Curie temperature of the amorphous intergranular phase as a function of the crystalline fraction.

iron nuclei located in those regions. In contrast, the high-field component should be assigned to Fe essentially surrounded by Fe, Co, B and Si located in the 'bulk' of the intergranular region, i.e. far from the crystalline grains.

For a given x_c, the peak position of the low-field Gaussian is independent on the Co content, while the peak position of the high-field Gaussian is shifted to higher values for $x = 60$ with respect to the values corresponding to $x = 0$ and 13.5. Therefore it can be concluded that the Co atoms surround preferentially Fe atoms located in the intergranular region far from the grains. Both peaks shift to smaller values as the crystallization fraction increases, as a result of the decrease of the Fe content of the residual amorphous phase as the nanocrystallization progresses, as previously pointed out.

3.3. Thermomagnetic measurements

The Curie temperature of the as-cast alloys (table 1) increases as the Co content in the alloy increases. Figure 5 shows the evolution of T_C for the residual amorphous phase as nanocrystallization progresses. For the Fe-rich alloy, T_C increases, in a similar way to that found for Finemet alloys, whereas for the Co-rich alloy, it strongly decreases with the crystalline fraction.

The decrease of the T_C of the residual amorphous phase of the Co-rich alloy with the annealing time can be explained in terms of composition. In fact, both the presence of refractory elements and the increase of the metalloid content lower T_C [35–37]. However, in the case of the Fe-rich alloy, the increase of the Curie temperature of the residual amorphous phase

with annealing time should be associated with the progressive lowering in the Si content of the amorphous phase, but other effects such as the magnetic interaction between the amorphous matrix and the nanocrystals should also be taken into account [38].

4. Conclusions

The compositions of both the residual amorphous phase and the Fe, Co, Si nanocrystalline grains of two Fe–Co nanocrystalline alloys, at different crystallization stages, were determined from combined ^{57}Fe Mössbauer spectrometry and XRD measurements. Significant differences between the values of the crystalline fraction obtained from the XRD and the Fe atomic fraction obtained by the MS are found for the Co-rich nanocrystalline alloys. The Co content of the nanocrystalline phase was found to be the same as that of the as-cast alloy. The hyperfine magnetic field distribution of the intergranular phase shows the emergence of a bimodal behaviour that can be described by means of two Gaussian components. This behaviour is consistent with a two-cluster-like model and can be attributed to the presence of iron-rich and iron-poor zones located in the bulk of the intergranular region and at the periphery of the crystalline grains, respectively. The analysis of the peak position of the two Gaussians permits us to conclude that Co atoms preferentially surround Fe atoms located in the intergranular region far from the grains. The difference in evolution of the Curie temperature of the intergranular matrix as the nanocrystallization progresses between alloys with low and high Co contents is associated at least partially with the changes in the Si content of the amorphous matrix with the crystalline fraction.

Acknowledgments

The authors thank Dr Rodriguez Pierna from the University of the Basque Country for supplying the ribbons. This work was partially supported by the DGES of the Spanish Ministry of Education (Project PB97-1119-CO2-01) and the PAI of the Junta de Andalucía and by the Picasso French–Spanish Programme (HF 1998-0211).

References

[1] Herzer G 1989 *IEEE Trans. Magn.* **25** 3327
[2] Herzer G 1992 *J. Magn. Magn. Mater.* **112** 93
[3] Yoshizawa Y, Oguma S and Yamauchi K 1988 *J. Appl. Phys.* **64** 6044
[4] Quintana P, Amano E, Valenzuela R and Irvine J T S 1994 *J. Appl. Phys.* **75** 6940
[5] Müller M, Grahl H, Mattern N, Kühn U and Schnell B 1996 *J. Magn. Magn. Mater.* **160** 284
[6] Willard M A, Laughlin D E, McHenry M E, Thoma D, Sickafus K, Cross J O and Harris V G 1998 *J. Appl. Phys.* **84** 6773
[7] Borrego J M, Conde C F, Conde A, Peña-Rodríguez V A and Greneche J M 2000 *J. Phys.: Condens. Matter* **12** 8089
[8] Borrego J M, Conde C F, Conde A and Greneche J M 2001 *J. Non-Cryst. Solids* **287** 120
[9] Conde C F and Conde A 1998 *Mater. Sci. Forum* **269–72** 719
[10] Brand R A, Lauer J and Herlach D M 1983 *J. Phys. F: Met. Phys.* **12** 675
[11] Greneche J M 1997 *Hyperfine Interact.* **110** 81
[12] Borrego J M, Conde A, Peña-Rodríguez V A and Greneche J M 2000 *Hyperfine Interact.* **131** 67
[13] Young A and Wiles D B 1982 *J. Appl. Crystallogr.* **15** 430
[14] *A Handbook of Lattice Spacings and Structures of Metals and Alloys* 1964 ed W B Pearson (Oxford: Pergamon)
[15] Kubaschewski O 1982 *Iron-Binary Phase Diagrams* (Berlin: Springer)
[16] Ruwali K, Gupta A, Kane S N and Duhaj P 1997 *Mater. Sci. Eng.* A **226–8** 729
[17] Vincze I 1978 *Solid State Commun.* **25** 689
[18] Narita K, Yamasaki J and Fukunaga H 1978 *IEEE Trans. Magn.* **14** 1016

[19] Dey S, Deppe P, Rosenberg M, Luborsky F E and Walter J L 1981 *J. Appl. Phys.* **52** 1805
[20] Mostafa M A, Balogh J and Kuzmann E 1986 *Phys. Status Solidi* a **96** 445
[21] Kopcewicz M, El Zayat M and Gonser U 1988 *J. Magn. Magn. Mater.* **72** 119
[22] Gupta A, Kane S N, Kraus L and Duhaj P 1995 *J. Magn. Magn. Mater.* **140–4** 321
[23] Fernández-Gubieda M L, Barandiaran J M, Plazaola F, Hernando A and Mobilio S 1992 *J. Non-Cryst. Solids* **151** 51
[24] Fernández-Gubieda M L, Orue I, Barandiaran J M and Plazaola F 1997 *Non-Crystalline and Nanoscale Materials* ed R Rivas and M A López Quintela (Singapore: World Scientific) p 172
[25] Plazaola F, Orue I, Fernández-Gubieda M L and Barandiaran J M 1995 *J. Appl. Phys.* **77** 3338
[26] Stearns M B 1963 *Phys. Rev.* **129** 1136
[27] Rixecker G, Schaaf P and Gonser U 1993 *Phys. Status Solidi* a **139** 309
[28] Randrianantoandro N, Gaffet E, Mira J and Greneche J M 1999 *Solid State Commun.* **111** 323
[29] Hampel G, Pundt A and Hesse J 1992 *J. Phys.: Condens. Matter* **4** 3195
[30] Gupta A, Ruwali K, Paul N and Duhaj P 2001 *Mater. Sci. Eng.* A **304–6** 371
[31] Zhang Y, Blázquez J S, Conde A, Warren P J and Cerezo A 2002 *Mat. Sci. Eng.* A at press
[32] Miglierini M 1994 *J. Phys.: Condens. Matter* **6** 1431
[33] Stearns M B 1973 *Phys. Rev.* B **8** 4383
[34] Hono K, Hiraga K, Wang Q, Inoue A and Sakurai T 1992 *Acta Metall. Mater.* **40** 2137
[35] Nielsen H J V and Nielsen O V 1981 *Proc. Conf. on Metallic Glasses: Science and Technology, (Budapest, 1980)* vol 2, ed F Hargitai, I Bakonyi and T Kemeny (Budapest: Central Research Institute for Physics) p 95
[36] Nielsen O V and Nielsen H J V 1980 *Solid State Commun.* **35** 281
[37] Kohmoto O, Ohya K, Yamauchi N, Fujishima H and Ojima T 1979 *J. Appl. Phys.* **50** 5054
[38] Borrego J M, Conde C F and Conde A 2000 *Phil. Mag. Lett.* **80** 359